Cardiel-Alvarez, M. A., Arnaltes, S., Rodriguez-Amenedo, J. L. & Nami, A. (2018). Decentralized Control of Offshore Wind Farms Connected to Diode-Based HVdc Links. *IEEE Transactions on Energy Conversion*, 33(3), pp. 1233–1241.

DOI: 10.1109/tec.2018.2804662

Decentralized Control of Offshore Wind Farms Connected to Diode-based HVDC Links

Miguel Ángel Cardiel-Álvarez, Santiago Arnaltes, Jose Luis Rodriguez-Amenedo, *Member, IEEE,* and Ashkan Nami

***Abstract*—This paper presents a novel decentralized control for offshore wind farms connected to the onshore grid through a high voltage direct current link by means of a diode rectifier. The proposed control system is implemented in each wind turbine generator system (WTGS). The capacitor placed at the filter of the wind turbine front-end converter is used for the proposed control implementation. Frequency control is achieved by aligning the capacitor voltage vector along a reference axis rotating at the reference frequency. Then, a frequency-reactive power droop control allows the synchronization of all the WTGSs. On the other hand, this droop strategy also leads to total reactive power sharing among WTGSs without relying on communications. An additional secondary frequency control is also implemented to compensate the frequency deviation caused by the droop control. The proposed control system has been validated by simulation and results demonstrate the appropriate performance even during start-up and faults.**

***Index Terms*—Diode rectifier, offshore wind farm (OWF), frequency control, distributed control, HVDC transmission.**

I. Introduction

RENEWABLE energies are growing year by year worldwide. Greenhouse-gas emissions are a huge problem, so breakthroughs are needed for the future of energy. Large offshore wind farms (OWFs) are expected to be one of the most promising areas of renewable energy, but they will be located at long distances far from the shore and this will demand the use of high-voltage direct current (HVDC) transmissions over high-voltage alternating current (HVAC) [1].

Nowadays, voltage-source converter (VSC) technology is the technology employed for the HVDC connection of OWFs because of its ability to supply voltage and frequency to the isolated offshore grid. Nevertheless, there is an increasing interest in the use of diode rectifier stations in HVDC links for the connection of OWFs [2], [3], [4], since diode rectifiers present better performance in terms of efficiency, reliability, converter size and cost [5]. However, diode rectifiers require large harmonic filters and a voltage and frequency control in the offshore grid for enabling the rectifier commutation.

In the literature, voltage and frequency control for OWFs connected through LCC-based HVDC links can be classified in two different solutions: centralized and distributed. A central control implemented in an additional STATCOM connected to a thyristor rectifier station can be found in [6] and [7]. [8] uses a hybrid topology with a DC series connection of a 12-pulse diode rectifier and a VSC, that also performs active power filtering. The proposal in [9] allows for the operation of type-3 and type-4 wind turbine generator systems (WTGSs) with a diode rectifier station. Type-3 WTGSs are controlled as a voltage source and then conventional P/f and Q/V droops are employed for the parallel operation of the WTGSs.

Distributed control solutions with diode rectifier HVDC connection are usually studied with type-4 WTGSs because of their control flexibility compared to type-3 WTGSs. In [10] and [11], a single aggregated model in the OWF is used to propose the control strategy principles, extended in [12] to the distributed voltage and frequency control. This distributed proposal has some drawbacks. An indirect frequency control is proposed, which relies on many measurements through the OWF providing lack of robustness. On the other hand, the angle reference for the WTGS frequency control also relies on the measurement of the point of common coupling (PCC) angle, which is difficult to transmit in real time to the WTGSs. Moreover, using the back-end converter for controlling DC voltage and the front-end converter for the wind turbine (WT) power might have a significant impact on the WT loads. The control proposed in [12] has been used to study efficiency in [13], rectifier filter reduction in [14] and integration of the diode rectifier in VSC-based HVDC grids in [15] and [16]. The proposal in [2] uses a GPS signal to provide a common angular reference to both type-3 and type-4 WTGSs. The advantage over the previous proposal is that WT active power control is not affected. All WTGS current injections are synchronized while voltage magnitude is clamped by the rectifier. However, WTGS voltage angle cannot be controlled and therefore neither the reactive power. A droop control is introduced to overcome this drawback, but reactive power is still not equally shared, which may lead to WTGSs operation points which are out of limits. Moreover, with this control strategy the WTGS decoupled active and reactive power control is not achieved, since the reference axis is not aligned with the voltage vector. In [17], the auxiliary AC connection to onshore proposed in [2] is replaced by the connection to a close OWF with a VSC rectifier station. The control proposed in [3] uses P/V and Q/f droops for the WTGSs parallel operation. Reactive power sharing among WTGSs without the need of communications is achieved. Nevertheless, communications are needed for the control itself, because WTGSs use a common angular position and frequency which are obtained from voltage measurement at a common point in the OWF grid, namely the PCC. Finally, another proposal with diode rectifier connection which is based on [18] is presented in [4]. This solution is not completely decentralized because it uses current set point values based on central and distributed measurements [18].

The authors are with the Department of Electrical Engineering, Carlos III University of Madrid, Madrid 28911, Spain (e-mail: mcardiel@ing.uc3m.es; amenedo@ing.uc3m.es; arnalte@ing.uc3m.es; anami@ing.uc3m.es).

This paper proposes a novel decentralized frequency control for OWFs connected to an HVDC link through a diode rectifier station. It allows the synchronization of all the WTGSs while reactive power is equally shared without the need of communications. The control at each WTGS is based on the voltage across the capacitor of the front-end converter filter. On the one hand, one important advantage is that frequency control does not rely on active power which means that the WTGS active power control channel is not used for this purpose allowing the classical WT active power control, *i.e.*, maximum energy yield. On the other hand, the reactive power control channel is used to align the voltage vector at the aforementioned capacitor with the reference axis of each WTGS. Besides this low-level control strategy, the synchronization among all WTGSs is achieved by affecting the individual reference axis through a droop between frequency and reactive power at each WTGS (f/Q droop). This guarantees both the synchronization required for the frequency control and the equal reactive power sharing among all the WTGSs of the OWF. Equally sharing reactive power is an important goal as the reactive power demanded by the OWF and the diode rectifier station can be very high and therefore it can only be satisfied if all WTGSs share the total reactive demand. Otherwise, converters can easily reach operation points which are out of their capability limits.

The above droop control makes the steady-state frequency of the system vary between acceptable frequency limits. Note that both the acceptable frequency deviations and the reactive power demanded by the OWF, which depends on the total active power flowing through the HVDC link, are taken into account to set the droop gain. Although the resulting frequency deviation is acceptable, an additional secondary frequency control is also proposed in this paper which allows eliminating the frequency error while keeping the equal reactive power sharing objective.

The paper is organized as follows. The two control fundamentals on which the proposal is based are addressed and analyzed in Section II. These studies are performed using simplified OWF equivalents with one and two aggregated WTGSs. Then, Section III presents the proposed decentralized control, introducing also the secondary regulation. In Section IV, simulation results of an OWF with six aggregated WTGSs are presented, showing system start-up, operation and fault response. Finally, conclusions are addressed in Section V.

II. Control Fundamentals

The decentralized control proposed in this study is based on two control principles: the direct frequency control (DFC) and a reactive power sharing strategy (QSS). Both control principles are presented in the following subsections using two OWF layouts. First, a single aggregated WTGS placed at the PCC is employed to analyze the DFC. Then, an OWF equivalent with two aggregated WTGSs is used to study the reactive power strategy.

A. Direct Frequency Control

The DFC strategy is explained through the equations of the system shown in Fig. 1. This system consists of a reduced representation of an OWF connected to the HVDC link through a diode rectifier station. The onshore inverter is operated in DC voltage mode and it can be a VSC, so it is represented by the DC source V_{di}, while the link is represented by its resistance R_{dc}. The diode rectifier DC voltage and current are V_{dr} and I_{dc1}, respectively, and the rectifier transformer is depicted by its short-circuit reactance X_t. P_r and Q_r are the active and reactive power drawn by the rectifier from the PCC. At this point, the OWF is represented by the active and reactive power generated by a single aggregated WTGS (P_g and Q_g) connected to the PCC bus. The capacitor C placed at the PCC represents both the capacitance of the harmonic filters at fundamental frequency and the reactive power compensation bank.

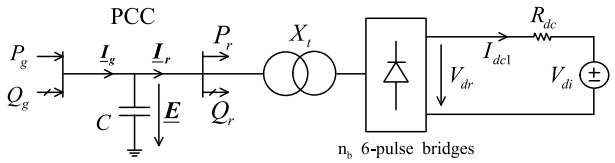

Fig. 1. Study case for the direct frequency control.

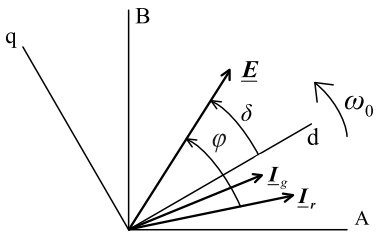

Fig. 2. Vector diagram in the stationary and synchronous reference systems.

The PCC voltage vector is denoted by $\underline{\boldsymbol{E}}$. Vectors $\underline{\boldsymbol{I_g}}$ and $\underline{\boldsymbol{I_r}}$ represent the wind farm and rectifier currents, respectively, expressed in the dq synchronous reference frame depicted in Fig. 2. The stationary frame is also depicted in Fig. 2, where ω_0 is the synchronous axis angular frequency, δ is the angle of $\underline{\boldsymbol{E}}$ and φ is the angle between $\underline{\boldsymbol{I_r}}$ and $\underline{\boldsymbol{E}}$.

The dynamic equation of the capacitor voltage vector $\underline{\boldsymbol{E}}$ expressed in the dq synchronous reference frame [12] is as follows:

$$\begin{aligned} I_{gd} - I_{rd} &= C\frac{dE_d}{dt} - \omega_0 C E_q \\ I_{gq} - I_{rq} &= C\frac{dE_q}{dt} + \omega_0 C E_d \end{aligned} \tag{1}$$

where d and q subscripts refer to the corresponding vector components.

Considering the per-unit representation, (1) becomes (2). Note that lower-case notation denotes per-unit representation of the variables along the paper.

$$\begin{aligned} \frac{b_c}{\omega_0}\frac{de_d}{dt} &= i_{gd} - i_{rd} + b_c e_q \\ \frac{b_c}{\omega_0}\frac{de_q}{dt} &= i_{gq} - i_{rq} - b_c e_d \end{aligned} \tag{2}$$

where $b_c{=}\omega_0 C Z_{base,ac}$ is the susceptance of C. Base values are detailed in Appendix A.

Applying the transformation from Cartesian coordinates to polar coordinates ($e_d{=}e\cos\delta$ and $e_q{=}e\sin\delta$) voltage angle δ

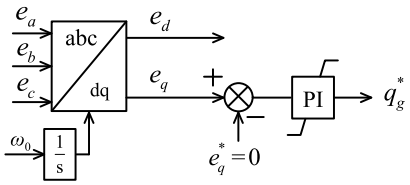

Fig. 3. Voltage q-component to zero control.

and magnitude e become the new state variables. The dynamic equations of the new state variables are presented in (3) and (4). For the sake of clarity, these equations are obtained in Appendix B.

$$\frac{b_c e^2}{\omega_0}\frac{d\delta}{dt} = -q_g + q_r - q_c \quad \Rightarrow \quad \frac{\omega}{\omega_0} = \frac{-q_g + q_r}{q_c} \tag{3}$$

$$\frac{b_c e}{\omega_0}\frac{de}{dt} = p_g - p_r \tag{4}$$

where p_g and q_g are the generated active and reactive power, while p_r and q_r are the corresponding active and reactive power drawn by the rectifier and transformer. Also, $\omega{=}\omega_0{+}\frac{d\delta}{dt}$ and the reactive power generated by C is $q_c{=}b_c e^2$.

On the one hand, frequency has to be controlled in the OWF in order to make the commutation of the diode rectifier possible. Since the synchronous axis in Fig. 2 is directly obtained by the desired OWF reference frequency ω_0, aligning voltage vector with the synchronous axis will lead to frequency control. Thus, angle δ needs to be controlled. Moreover, it should be pointed out that the synchronous reference ω_0 is not affected by any grid disturbance or measurement noise, given that it is obtained directly from a reference signal.

According to (3), variations of the voltage angle δ depend on the reactive power balance at the capacitor bus. Therefore, q_g can be used to control δ. Particularly, aligning the voltage vector implies making the voltage q-component (e_q) zero. This target is shown in the control channel at the bottom of Fig. 3, where a proportional-integral (PI) controller is used to get the required reactive power reference q_g^*.

On the other hand, (4) shows that the active power balance at the capacitor bus (PCC) drives the dynamics of the voltage magnitude e. If there is a positive imbalance ($p_g{>}p_r$), e will increase. This will make the rectifier DC voltage v_{dr} increase and so p_r, as the onshore inverter DC voltage is fixed, until power balance is achieved at a certain voltage magnitude. Therefore, the voltage magnitude is clamped by the HVDC link voltage and does not need to be controlled as it will be demonstrated following and it will be shown in the simulation results.

The DFC is analyzed by considering small-signal increments around a steady-state point in order to demonstrate these control principles. By linearizing (4):

$$\frac{b_c e_0}{\omega_0}\frac{d\Delta e}{dt} + k_{p,link}\Delta e = \Delta p_g \tag{5}$$

where the expression $k_{p,link}\Delta e{=}\Delta p_r$ is detailed in Appendix C and subscript 0 stands for steady-state value.

In (5), it is demonstrated that the OWF active power is completely drawn by the HVDC link in steady-state, since

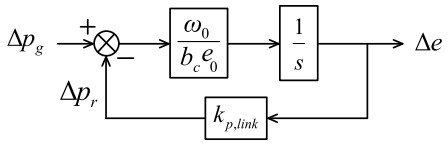

Fig. 4. Block diagram according to (5).

$\Delta p_r{=}\Delta p_g$. According to (5), there is a first order transfer function between the voltage magnitude increment Δe and the generated active power increment Δp_g. Also, the gain of this transfer function shows that a large increment of the generated active power will produce a small increment of the voltage magnitude. This is shown in the block diagram of Fig. 4. Note that Δp_g is the independent input of the system, which mainly depends on the wind. Therefore, this demonstrates why e does not need to be controlled because it is clamped between certain limits corresponding to the minimum and maximum active power transmitted through the link.

The small-signal study is also applied to (3). As the equation includes the increment of the generated reactive power (Δq_g), the equation of the controller in Fig. 3 should also be considered: $\Delta e_q = \Delta(e\sin\delta) = \Delta e\sin\delta_0 + e_0\cos\delta_0\Delta\delta = e_0\Delta\delta$, thus $\Delta q_g = e_0(k_p^f\Delta\delta + k_i^f\omega_0\int\Delta\delta dt)$ (where k_p^f and k_i^f are the proportional and integral parameters of the PI, respectively). After operating, the final equation obtained is as follows:

$$\frac{b_c e_0}{\omega_0^2}\frac{d^2\Delta\delta}{dt^2} + \frac{k_p^f}{\omega_0}\frac{d\Delta\delta}{dt} + k_i^f\Delta\delta = \frac{k_{q,link} - 2b_c e_0}{b_c e_0}(\Delta p_g - k_{p,link}\Delta e) \tag{6}$$

where $k_{q,link}$ is detailed in Appendix C. Note that this equation is similar to the swing equation of a synchronous generator.

The study of the classical model of a synchronous generator connected to an infinite bus [19] leads to the following swing equation:

$$\frac{2H}{\omega_0}\frac{d^2\Delta\delta'}{dt^2} + \frac{D}{\omega_0}\frac{d\Delta\delta'}{dt} + k_s\Delta\delta' = \Delta p_m \tag{7}$$

where H is the inertia constant, $D{=}\frac{k_D}{\omega_0}$ being k_D the damping torque coefficient and $k_s{=}\frac{e'_0 u_\infty\cos\delta'_0}{x_{eq}}$ the synchronizing torque coefficient. e' and δ' are the generator voltage magnitude and angle, respectively; and u_∞ is the infinite bus voltage magnitude with angle equal to zero. x_{eq} is the total reactance between e' and the infinite bus, and p_m is the mechanical power supplied to the generator.

By comparing (6) and (7), it is observed that the independent term of the equation depends on the power input of each system, given the relationship in (5). Moreover, the correspondence between the terms in the equations is as follows:

$$H = \frac{b_c e_0}{2\omega_0} \quad ; \quad D = k_p^f \quad ; \quad k_s = k_i^f \tag{8}$$

As stated in (8), the inertia of the system in Fig. 1 is due to C and it is of a lower magnitude order than the inertia constant of a synchronous generator. In addition, the DFC gains k_p^f

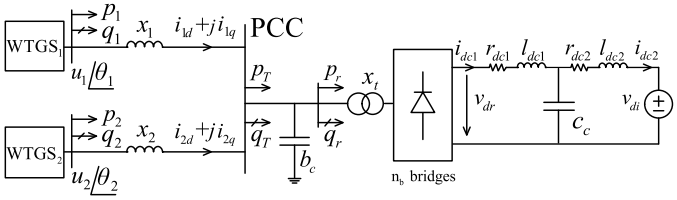

Fig. 5. Study case for the reactive power strategy.

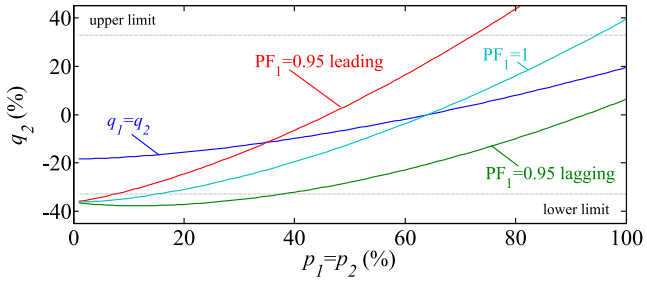

Fig. 6. Steady-state reactive power of $WTGS_2$ under different reactive power strategies in $WTGS_1$ for a swept in active power level.

and k_i^f provide a damping and a synchronizing torque to the system, correspondingly. The fact that there is an equivalent synchronizing torque proves the ability of the proposed control system to achieve the alignment of the capacitor voltage vector along the synchronous reference frame in a stable way. It should be pointed out that k_p^f will take higher values than the damping coefficient in a synchronous generator, so the system becomes well damped.

B. Reactive Power Control Strategy

This subsection deals with the steady-state analysis of an OWF in order to justify the need of a reactive power sharing strategy among WTGSs. For the sake of clarity, zero subscript for steady-state will be omitted in this subsection.

The analyzed study case is the one shown in Fig. 5. There are two aggregated WTGSs rated 225 MVA and generating an active power equal to p_k and a reactive power equal to q_k (subscript k stands for $WTGS_1$ and $WTGS_2$ in this subsection). Each wind turbine bus has a voltage vector magnitude and angle equal to u_k and θ_k, respectively. Each WTGS injects the current vector $(i_{kd}+ji_{kq})$ through the line connected to the PCC. This line is represented by x_k, taking the transformer short-circuit reactance and the line reactance into consideration. The PCC voltage is considered to be the angle reference ($e\angle 0°$) and the sum of the incoming active and reactive power from the WTGSs is depicted by p_T and q_T, respectively. The PCC capacitance, the rectifier transformer, the diode rectifier and the onshore inverter DC voltage source are equal to the ones considered in Section II-A (Fig. 1). The DC cable is represented by the T-equivalent circuit composed of resistances r_{dc1} and r_{dc2}, inductances l_{dc1} and l_{dc2}, and capacitance c_c. The parameters used are depicted in Appendix D.

This subsection seeks to analyze the steady-state for given powers p_1 and p_2. Because of the lack of losses in the OWF model considered until now, (9) can be derived and the stationary equations (C.1) to (C.6) depicted in Appendix C can be solved considering r_{dc}=r_{dc1}+r_{dc2}. This equations together with (10) lead to find the values of e, i_{1d}, i_{2d} and q_T. Besides, u_{1q} and u_{2q} are obtained in (11) according to the zero angle of PCC voltage vector.

$$p_T = p_r = p_1 + p_2 = ei_{1d} + ei_{2d} \tag{9}$$

$$q_T = q_r - b_c e^2 \tag{10}$$

$$u_{kq} = x_k i_{kd} \qquad (k = 1, 2) \tag{11}$$

Consequently, there are still six unknown variables: u_{kd}, i_{kq} and q_k. However, there are only 5 equations:

$$\begin{aligned} q_k &= u_{kq} i_{kd} - u_{kd} i_{kq} \qquad (k = 1, 2) \\ u_{kd} &= e - x_k i_{kq} \qquad (k = 1, 2) \\ q_T &= -e(i_{1q} + i_{2q}) \end{aligned} \tag{12}$$

Hence, one of the variables has to be fixed and the others can then be obtained. This means that if one reactive power is predetermined, the other will be the one required to close the OWF reactive balance at any active power level. This approach is not robust because it can lead to exceeding the reactive limits of the WTGS. If this study was accomplished for an OWF with more than two WTGSs, the result would be that it is possible to set the reactive power of all WTGSs except one that has to close the reactive power balance.

Fig. 6 shows the values of q_2 as function of the active power generated by the WTGSs from zero to full power using different reactive power strategies in q_1. Specifically, $WTGS_1$ is tested with power factor (PF_1) equal to 1, 0.95 leading, 0.95 lagging and with the reactive power sharing strategy (q_1=q_2). Fig. 6 is obtained by solving the system with equations (C.1) to (C.6), (9) to (12) and the equation that determines the value of q_1 in each of the strategies. Moreover, the reactive power limits, set to $\pm 32.87\%$ (0.95 power factor at rated power), are also depicted in Fig. 6. Note that all per-unit powers shown in figures along the paper use WTGS rating as base power.

As it can be observed in Fig. 6, following conventional reactive power strategies is not acceptable because it would force the WTGS to exceed the reactive limits. Note that this issue would be even more pronounced in a real OWF with tens of WTGSs. It should also be pointed out that the cases presented in Fig. 6 lead to voltage magnitudes at the WTGSs terminals between acceptable values (0.9 p.u. and 1.1 p.u.) [20].

However, the QSS maintains the voltages and reactive-power values within limits and provides a single steady-state solution in the OWF, thus it is the most appropriated strategy. It implies that all WTGSs will contribute to close the reactive power balance, but not only one.

III. Decentralized Control

This section describes the decentralized control proposed in this paper. Firstly, the WTGS control is detailed. Then, the WTGSs synchronization strategy is presented in order to

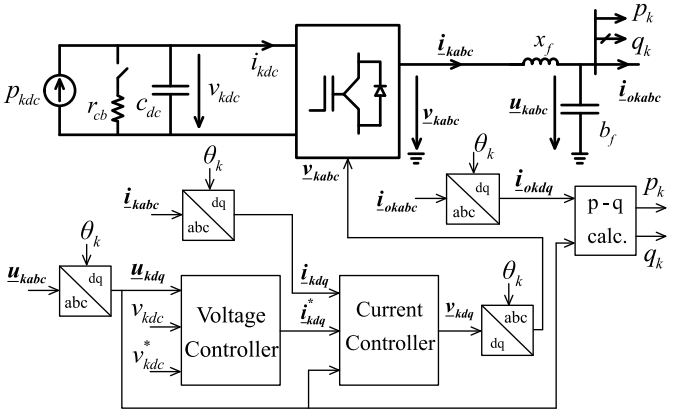

Fig. 7. Control of the WTGS front-end converter.

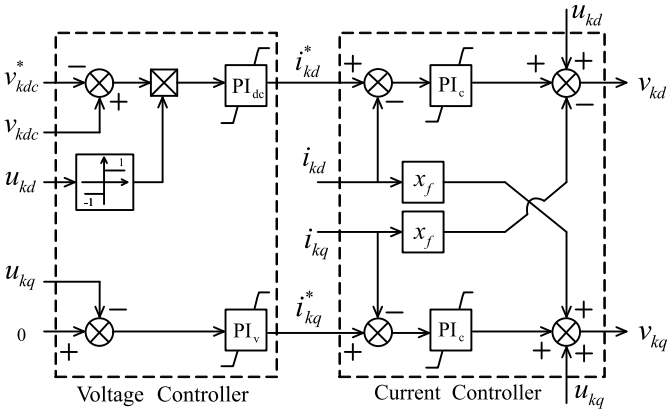

Fig. 8. Voltage and current inner controllers of the front-end converter.

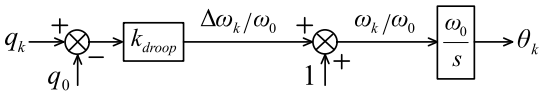

Fig. 9. Control scheme of the decentralized control.

accomplish the proposed decentralized control. Finally, the secondary control is described, given that it can provide an additional control feature.

A. Front-End Converter Control

The WTGSs front-end converter is depicted at the top of Fig. 7, where subscript k is the WTGS number. The incoming active power from the back-end converter of the WTGS (p_{kdc}) is the input to the DC link of the front-end converter. v_{kdc} is the DC link capacitor (c_{dc}) voltage and i_{kdc} is the DC current drawn by the front-end converter. In addition, overvoltage protection is provided by a crowbar with resistance r_{cb}. The output filter consists of a series inductor (reactance x_f) and a parallel capacitor (susceptance b_f).

The notation for AC voltages and currents uses subscript abc for the corresponding three-phase representation. The front-end converter and the WTGS currents are denoted by i_k and i_{ok}, respectively, and voltage at the WTGS bus is u_k. Active and reactive powers p_k and q_k are calculated by means of $\underline{\boldsymbol{u}}_{\boldsymbol{k}}$ and $\underline{\boldsymbol{i}}_{\boldsymbol{ok}}$ (as $p_k{=}u_{kd}i_{okd}{+}u_{kq}i_{okq}$ and $q_k{=}u_{kq}i_{okd}{-}u_{kd}i_{okq}$).

The front-end converter control is based on the DFC detailed in Section II-A. The controlled voltage vector is $\underline{\boldsymbol{u}}_{\boldsymbol{k}}$, being θ_k the angle obtained by integrating the frequency ω_k which will be obtained in Section III-B and Section III-C.

The voltage and current controllers in Fig. 7 are depicted in Fig. 8, where two control channels can be observed. The d-component channel is based on the conventional control of v_{kdc} to supply the incoming power through the front-end converter. As the control can reach zero u_{kq} with negative u_{kd}, v_{kdc} error sign is properly adjusted. $\mathrm{PI_{dc}}$ and $\mathrm{PI_c}$ controllers are used for voltage and current control, respectively. Note that keeping unchanged the power control channel is one of the objectives of the proposed control strategy. The q-component channel seeks to align $\underline{\boldsymbol{u}}_{\boldsymbol{k}}$ with the d reference axis of the WTGS, thus $u_{kq}{=}0$. Therefore, the q voltage controller provides the reactive current reference i^*_{kq} through $\mathrm{PI_v}$ controller. Control parameters are detailed in Appendix D.

B. Wind Turbine Generator Systems Synchronous Operation Control

In the DFC detailed in Section II-A, there was only one aggregated WTGS controlling frequency and angle. However, in an OWF there are tens of WTGSs and synchronous operation is required. As it will be shown, QSS will produce the right angle differences among the WTGS bus voltages and, therefore, the same frequency.

WTGSs synchronous operation strategy uses the f/Q droop shown in Fig. 9. In order to synchronize all the WTGSs, a frequency increment over ω_0 is added as a function of the WTGS reactive power increment. Note that ω_0 is an internal constant value of the controller which is equal to the reference frequency of the system.

The increment of frequency over the reference is obtained as the product of the constant k_{droop} and the difference $q_k{-}q_0$. In order to obtain equal reactive power sharing, q_0 and k_{droop} are the same in all the WTGSs, while θ_k is the angle used in the dq transformations in Fig. 7. The angle differences will change during transients until they reach a steady-state value. Hence, the proposed control strategy reaches WTGSs synchronous operation (equal $\Delta\omega_k$) and the right angle differences while leading to the QSS (equal q_k) without the need of a communication channel.

As a proof of concept, the system in Fig. 5 is simulated under the decentralized control. In the simulation, performed in MATLAB/Simulink, dynamic models of the WTGSs and the HVDC link are used, while an average-value model of the diode rectifier [21] is employed and the OWF grid is modelled at the fundamental frequency [22]. Both WTGSs are initially generating 0.5 p.u. of active power. Then, active power changes are scheduled at t=0.1 s (Δp_{1dc}=0.25 p.u. and Δp_{2dc}=-0.5 p.u.) and at t=2.5 s (Δp_{1dc}=0.25 p.u. and Δp_{2dc}=1 p.u.).

Results are shown in Fig. 10. As it can be observed, the reactive power sharing among the WTGSs is achieved in steady-state. In addition, WTGSs also achieve synchronous operation and frequency deviation is within acceptable limits [20]. Voltage magnitudes, which vary with the active power transmitted through the HVDC link, are clamped between

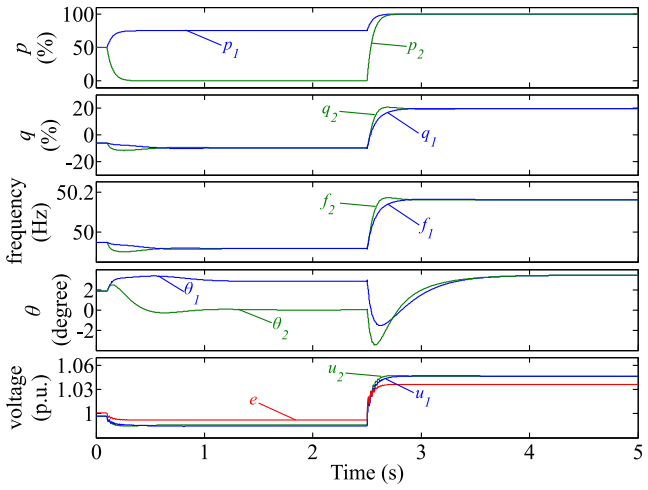

Fig. 10. WTGSs active and reactive power, frequency, voltage angle and magnitude in the OWF of Fig. 5 under decentralized control.

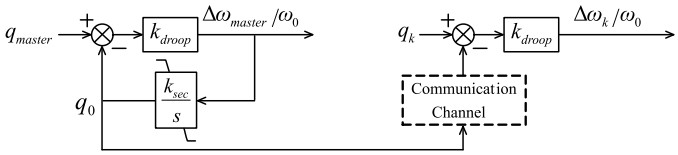

Fig. 11. Control scheme of the decentralized control with secondary regulation.

0.95 p.u and 1.05 p.u. Fig. 10 shows that the higher the active power generated, the higher the reactive power level of the WTGSs and the higher the voltage magnitudes in the grid. Moreover, it can be observed that voltage angles at the WTGSs buses change during transients to achieve the values required by the OWF power flow. These simulation results demonstrate that the proposed control objectives are satisfactorily achieved.

C. Secondary Frequency Control

The decentralized control described in Section III-B will lead to frequency deviations. In this section, a secondary control is proposed to achieve constant frequency if required.

For the secondary control, a master WTGS is assigned which generates a reference signal q_0 that is sent to the other WTGSs in order to drive frequency to its nominal value. Specifically, reactive power reference q_0 is generated through an integral control with constant k_{sec} as it is shown in Fig. 11. The other WTGSs will receive the signal q_0 generated by the integral controller through a communication channel.

The decentralized control with secondary regulation has also been simulated for the system of Fig. 5. The system is simulated under the same conditions established in Section III-B. The communication channel is simulated as a time delay of 0.1 s and results are presented in Fig. 12.

This strategy ensures the synchronous operation and reactive power sharing in steady-state operation while achieving constant frequency. Communication among WTGSs is needed and the dynamics of the system is slower than in the decentralized control shown in Fig. 10, due to the integral secondary control and the communication delay.

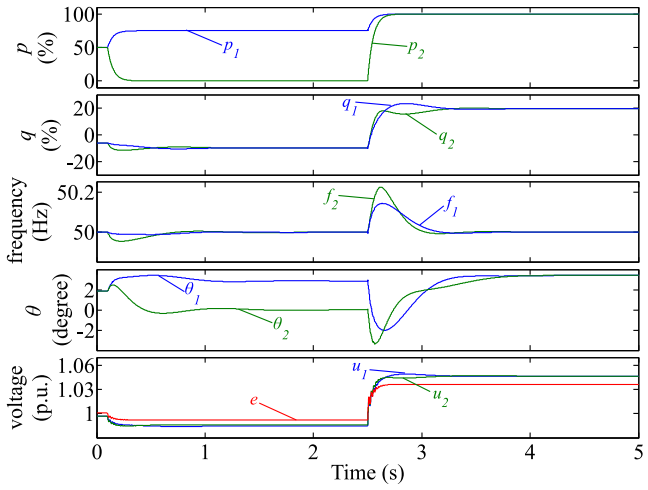

Fig. 12. WTGSs active and reactive power, frequency, voltage angle and magnitude in the OWF of Fig. 5 under decentralized control with secondary regulation.

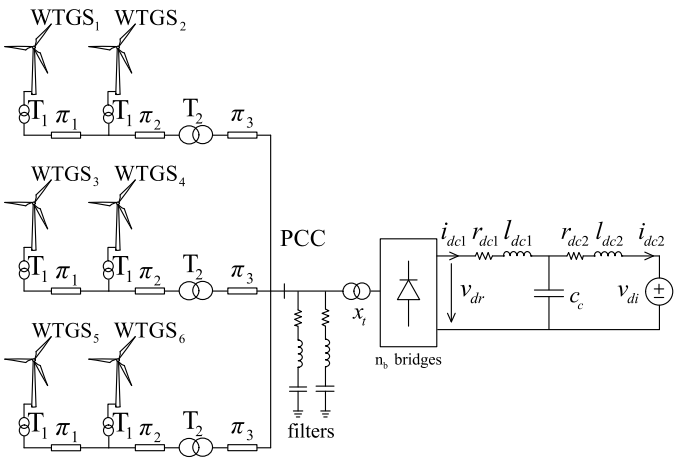

Fig. 13. Study case.

IV. Simulation Results

After the proof of concept in Section III, the OWF grid layout shown in Fig. 13 is used for simulation studies. It represents an equivalent of an OWF with 90 WTGSs rated 5 MW (3 clusters with independent line feeders and 3 strings with 10 WTGSs), but using six aggregated WTGSs rated 75 MVA. The WTGS model has been described in Section III-A and transformers are modelled by their short-circuit impedance $r_{Tk}+jx_{Tk}$ (being k the identification number of the transformer). T_1 steps up from 0.69 kV to 33 kV and T_2 from 33 kV to 220 kV. AC cables are modelled by a π-model and parameters are detailed in Appendix D.

Steady-state analysis has been performed to check that operation points are within limits. At full load, reactive power supplied by each WTGS is 0.205 p.u. and the highest voltage magnitude in the OWF is 1.077 p.u. At low load, WTGSs have to absorb a reactive power of 0.2607 p.u. while the lowest voltage magnitude reached is 0.9107 p.u. Therefore, variables are between acceptable operation limits [20].

This study case will be simulated in this section by using the electromagnetic transients program PSIM. Start-up procedure

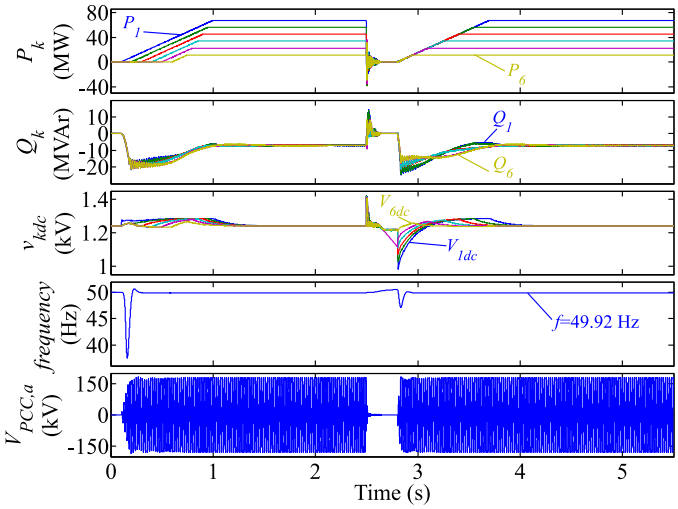

Fig. 14. WTGSs active power, reactive power and DC-bus voltage, PCC frequency and phase voltage responses to start-up procedure and fault under decentralized control.

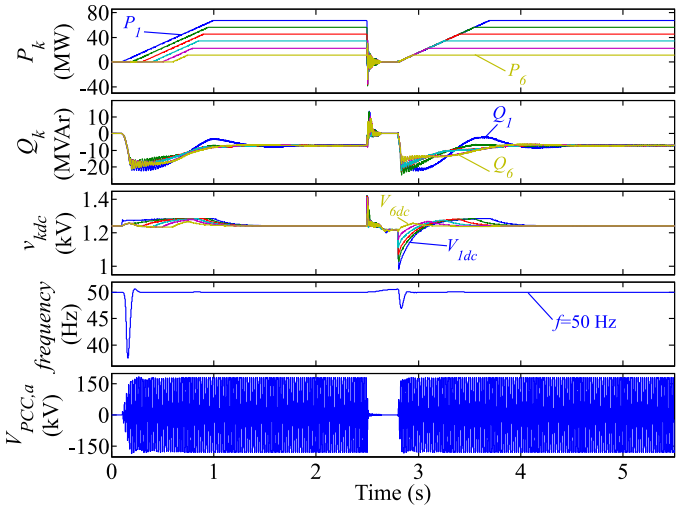

Fig. 15. WTGSs active power, reactive power and DC-bus voltage, PCC frequency and phase voltage responses to start-up procedure and fault under decentralized control with secondary regulation.

and short-circuit response are studied. For the start-up, at t=0.1 s, $WTGS_1$ DC voltage link starts receiving power from the back-end converter at a constant rate equal to 1 p.u./s. The same applies to the following WTGSs with a 0.1 s delay between their start-ups until they reach different active power operation points from 0.9 p.u. at $WTGS_1$ to 0.15 p.u. at $WTGS_6$ with increments of 0.15 p.u. among them (expressed in WTGS base). A 300-ms fault is scheduled at t=2.5 s at the PCC. The incoming active power to the front-end converter is driven to zero during the fault and then increases with a constant rate of 1 p.u./s once the fault is cleared. Current is controlled during the fault in order to provide the fault ride-through response of the WTGS. Moreover, crowbar overvoltage protection is activated when DC bus voltage is over 1.25 p.u. and remains active until voltage goes under 1.2 p.u.

First, simulation results without secondary regulation are presented in Fig. 14. This figure shows the system start-up, normal operation and fault ride-through. Before the fault, it can be observed that the proposed control is able to start-up the system, provided that the front-end converter DC bus is fed. The system reaches a steady-state operation at 49.92 Hz and all WTGSs share the demanded reactive power without exceeding their reactive limits. The short-circuit response mainly depends on the converter response to the voltage sag. The OWF recovers synchronous operation once the fault is cleared. Moreover, WTGS DC-link voltages show the crowbars actuation during the first milliseconds of the fault. PCC frequency is measured by means of a phase-locked loop (PLL), so it is affected by the PLL dynamics.

Then, the study case is simulated when using the secondary control. Master WTGS is $WTGS_1$ and the communication delay is equal to 0.1 s. Results, depicted in Fig. 15, show that frequency reaches the reference value (50 Hz) both after the start-up and after the fault. It should be pointed out that the secondary control slows down the system response due to the slow integral action, but WTGSs are able to start-up the grid, operate and recover voltage after the fault is cleared.

V. Conclusion

This paper has presented a novel decentralized control strategy for the synchronous operation of the WTGSs in an offshore wind farm connected to an HVDC link through a diode rectifier station. Frequency control is based on the alignment of the voltage vector with a reference axis. Frequency control relies on the reactive power and therefore it does not require using the WTGS power control channel, which is one of the objectives of the proposed control strategy. The synchronous operation is achieved by using a reactive-frequency droop, which adds a frequency increment as a function of the reactive power increment in each WTGS. On the other hand, this droop control also allows to achieve equal reactive power sharing among all the WTGSs, which is another objective to avoid reaching operation points which are out of limits. Moreover, an additional secondary regulation has also been proposed, which leads to constant frequency operation if required. Simulation results during start-up, normal operation and fault conditions validate the control proposal and demonstrate the appropriate performance of the controlled system.

Appendix A

Base magnitudes for the DC link are as follows (being n_b the number of 6-pulse diode bridges):

$$P_{base,dc} = S_{base,ac} = V_{base,dc} I_{base,dc} \tag{A.1}$$

$$V_{base,dc} = \frac{3\sqrt{2}}{\pi} n_b V_{base,ac} \; ; \; I_{base,dc} = \frac{\pi}{n_b \sqrt{6}} I_{base,ac} \tag{A.2}$$

$$R_{base,dc} = \frac{V_{base,dc}}{I_{base,dc}} = \left(\frac{3\sqrt{2}}{\pi} n_b \right)^2 Z_{base,ac} \tag{A.3}$$

APPENDIX B

The relationships between the derivatives of Cartesian and polar coordinates are as follows:

$$\frac{de_d}{dt} = \frac{d(e\cos\delta)}{dt} = \frac{e_d}{e}\frac{de}{dt} - e_q\frac{d\delta}{dt}$$
$$\frac{de_q}{dt} = \frac{d(e\sin\delta)}{dt} = \frac{e_q}{e}\frac{de}{dt} + e_d\frac{d\delta}{dt} \quad \text{(B.1)}$$

Then, by operating (B.1) we can obtain (B.2).

$$e^2\frac{d\delta}{dt} = -e_q\frac{de_d}{dt} + e_d\frac{de_q}{dt}$$
$$e\frac{de}{dt} = e_d\frac{de_d}{dt} + e_q\frac{de_q}{dt} \quad \text{(B.2)}$$

Different expressions of the active and reactive powers addressed in (3) and (4) are provided in (B.3).

$$p_g = e_d i_{gd} + e_q i_{gq}$$
$$q_g = -e_d i_{gq} + e_q i_{gd}$$
$$p_r = e_d i_{rd} + e_q i_{rq}$$
$$q_r = -e_d i_{rq} + e_q i_{rd}$$
$$q_c = b_c e^2 \quad \text{(B.3)}$$

By introducing the terms of (2) in (B.2) the following equations are obtained:

$$e^2\frac{d\delta}{dt} = \frac{\omega_0}{b_c}(-e_q i_{gd} + e_q i_{rd} - b_c e_q^2 + e_d i_{gq} - e_d i_{rq} - b_c e_d^2)$$
$$e\frac{de}{dt} = \frac{\omega_0}{b_c}(e_d i_{gd} - e_d i_{rd} + e_q i_{gq} - e_q i_{rq}) \quad \text{(B.4)}$$

Finally, by identifying the expressions in (B.3), (3) and (4) are obtained.

APPENDIX C

The equations which define the per-unit AC-DC conversion for the rectifier are [23]:

$$k_{\alpha,\mu} = \frac{1}{2}(\cos\alpha + \cos(\alpha+\mu)) \cdot \sqrt{1 + (\mu\csc\mu\csc\lambda - \cot\lambda)^2} \quad \text{(C.1)}$$

$$v_{dr} = k_{\alpha,\mu} e\cos\varphi = e\cos\alpha - r_\mu i_{dc1} \quad \text{(C.2)}$$

$$r_\mu i_{dc1} = \frac{e}{2}(\cos\alpha - \cos(\alpha+\mu)) \quad \text{(C.3)}$$

$$p_r = v_{dr} i_{dc1} \quad ; \quad q_r = p_r\tan\varphi \quad \text{(C.4)}$$

where $r_\mu = \frac{3X_t}{\pi R_{base,dc}} = \frac{\pi x_t}{6n_b}$ is the per-unit commutating resistance; α and μ are the firing and commutation angles, respectively; and $\lambda = 2\alpha+\mu = \mu$ ($\alpha = 0$ because of diodes).

For the sake of clarity, variable $k_{\alpha,\mu}$ is kept constant in this paper with a value equal to steady-state for the small-signal studies [23]. Considering Kirchhoff voltage law at the link shown in Fig. 1 ($v_{di} + r_{dc} i_{dc1} - v_{dr} = 0$) multiplied by i_{dc1} results in obtaining this current. Then, i_{dc1} can be introduced in (C.5) to obtain (C.6).

$$e = v_{di} + (r_\mu + r_{dc}) i_{dc1} \quad \text{(C.5)}$$

$$e = v_{di} + (r_{dc} + r_\mu)\left(-\frac{v_{di}}{2r_{dc}} + \frac{\sqrt{v_{di}^2 + 4r_{dc}p_r}}{2r_{dc}} \right) \quad \text{(C.6)}$$

TABLE I
PARAMETERS

Parameter	Value
Base	f_0=50 Hz $S_{base,ac}$=450 MVA $V_{base,ac}$=220 kV
x_t/n_b	0.12 p.u. (n_b=2 6-pulse bridges)
b_c	0.2 p.u.
r_{dck}	0.003186 p.u.=2.5 Ω $k = 1, 2$
l_{dck}	0.2 p.u.=0.5 H $k = 1, 2$
c_c	6.409 p.u.=26 μF
c_{dc}	0.15 p.u. of WTGS base
x_f	0.15 p.u. of WTGS base
b_f	0.05 p.u. of WTGS base
r_{cb}	20 mΩ
x_k	0.13 p.u. $k = 1, 2$
$x_{T1}/6$	0.07 p.u. (x_{T1}/r_{T1}=80) of transformer base
$x_{T2}/3$	0.1 p.u. (x_{T2}/r_{T2}=80) of transformer base
cable π_1	r=0.02826 p.u. x=0.03038 p.u. b=0.003011 p.u.
cable π_2	r=0.02776 p.u. x=0.0787 p.u. b=0.005237 p.u.
cable π_3	r=0.001882 p.u. x=0.0111 p.u. b=0.0642 p.u.
filter 1	R=0.3286 Ω L=0.0951 H C=0.8805 μF
filter 2	R=0.2774 Ω L=0.0679 H C=0.8805 μF
v_{di}	0.9654 p.u.
PI_{dc}	k_{dc}=3.5 p.u. of WTGS base τ_{dc}=0.15 s
PI_{v}	k_v=1 p.u. of WTGS base τ_v=0.15 s
PI_{c}	k_c=5 p.u. of WTGS base τ_c=0.005 s
k_{droop}	0.0167 p.u./p.u. of WTGS base (q_0=0 p.u.)
k_{sec}	300 p.u. of WTGS base s^{-1}

Then, taking the small-signal increments leads to (C.7). Note that subscript zero denotes the steady-state value for the variables.

$$\Delta p_r = k_{p,link}\Delta e \quad ; \quad k_{p,link} = \frac{\sqrt{v_{di}^2 + 4r_{dc}p_{r0}}}{r_{dc} + r_\mu} \quad \text{(C.7)}$$

The small-signal increments are also applied to (C.4):

$$\Delta q_r = \tan\varphi_0\Delta p_r + \frac{p_{r0}}{\cos^2\varphi_0}\Delta\varphi \quad \text{(C.8)}$$

where $\Delta\varphi$ can be derived from (C.2).

After introducing the equation of $\Delta\varphi$ in (C.8), the expression for Δq_r is as follows:

$$\Delta q_r = k_{q,link}\Delta e \quad \text{(C.9)}$$

where $k_{q,link} = \tan\varphi_0 k_{p,link} + \frac{2i_{dc0}r_\mu v_{di}}{e_0(r_{dc}+r_\mu)\sin(2\varphi_0)}$.

APPENDIX D

The parameters used for the different studies through the paper are detailed in Table I. Per-unit DC inductance and capacitance are $l_{dc} = \frac{\omega_0 L_{dc}}{R_{base,dc}}$ and $c_c = \omega_0 C_c R_{base,dc}$, respectively. Section IV considers the diode rectifier transformer resistance r_t (x_t/r_t=80).

PI controllers are given by their proportional gain k and time constant τ. Base voltage for the DC bus of the front-end converter is $V_{WTGSbase,dc} = 2\sqrt{2/3}V_{WTGSbase,ac}$ and per-unit DC capacitance is calculated as $c_{dc} = \omega_0 C_{dc}\frac{V_{WTGSbase,dc}^2}{P_{WTGSbase,dc}}$, being the nominal voltage and power the base values of the converter.

REFERENCES

[1] R. Perveen, N. Kishor, and S. R. Mohanty, "Off-shore wind farm development: Present status and challenges," *Renewable and Sustainable Energy Reviews*, vol. 29, pp. 780–792, 2014.

[2] C. Prignitz, H.-G. Eckel, S. Achenbach, F. Augsburger, and A. Schön, "Fixref: A control strategy for offshore wind farms with different wind turbine types and diode rectifier hvdc transmission," in *Power Electronics for Distributed Generation Systems (PEDG), 2016 IEEE 7th International Symposium on*. IEEE, 2016, pp. 1–7.
[3] A. A. Iván, P. G. Ruben, R. Blasco-Gimenez, and R. A. Javier, "Control strategy of a hvdc-diode rectifier connected type-4 off-shore wind farm," in *Future Energy Electronics Conference (IFEEC), 2015 IEEE 2nd International*. IEEE, 2015, pp. 1–6.
[4] S. Seman, R. Zurowski, and C. Taratoris, "Interconnection of advanced type 4 wtgs with diode rectifier based hvdc solution and weak ac grids," in *Proceedings of the 14th Wind Integration Workshop*, 2015.
[5] O. Saboro-Romano, A. Bidadfar, mer Gksu, M. Altin, N. Cutululis, and P. Srensen, "Connection of owpps to hvdc networks using vscs and diode rectifiers: an overview," 2016, poster presentation.
[6] S. Bozhko, G. Asher, R. Li, J. Clare, and L. Yao, "Large offshore dfig-based wind farm with line-commutated hvdc connection to the main grid: Engineering studies," *IEEE transactions on energy conversion*, vol. 23, no. 1, pp. 119–127, 2008.
[7] S. Foster, L. Xu, and B. Fox, "Control of an lcc hvdc system for connecting large offshore wind farms with special consideration of grid fault," in *Power and Energy Society General Meeting-Conversion and Delivery of Electrical Energy in the 21st Century, 2008 IEEE*. IEEE, 2008, pp. 1–8.
[8] T. H. Nguyen, D.-C. Lee, and C.-K. Kim, "A series-connected topology of a diode rectifier and a voltage-source converter for an hvdc transmission system," *Power Electronics, IEEE Transactions on*, vol. 29, no. 4, pp. 1579–1584, 2014.
[9] R. Vidal-Albalate, R. Pena, E. Belenguer, S. Ano-Villalba, R. Bernal-Perez, and R. Blasco-Gimenez, "Simultaneous connection of type-3 and type-4 off-shore wind farms to hvdc diode rectifier units," in *Proceedings of the 15th Wind Integration Workshop*, 2016, pp. 1–6.
[10] R. Blasco-Gimenez, S. Añó-Villalba, J. Rodríguez-D'derlée, F. Morant, and S. Bernal, "Voltage and frequency control of sg based wind farms with uncontrolled hvdc rectifier," in *Industrial Electronics (ISIE), 2010 IEEE International Symposium on*. IEEE, 2010, pp. 2499–2504.
[11] R. Blasco-Gimenez, S. Ano-Villalba, J. Rodriguez-D'Derlee, S. Bernal-Perez, and F. Morant, "Diode-based hvdc link for the connection of large offshore wind farms," *Energy Conversion, IEEE Transactions on*, vol. 26, no. 2, pp. 615–626, 2011.
[12] R. Blasco-Gimenez, S. Ano-Villalba, J. Rodriguez-D'Derlee, F. Morant, and S. Bernal-Perez, "Distributed voltage and frequency control of offshore wind farms connected with a diode-based hvdc link," *Power Electronics, IEEE Transactions on*, vol. 25, no. 12, pp. 3095–3105, 2010.
[13] S. Bernal-Perez, S. Ano-Villalba, R. Blasco-Gimenez, and J. Rodriguez-D'Derlee, "Efficiency and fault ride-through performance of a diode-rectifier-and vsc-inverter-based hvdc link for offshore wind farms," *IEEE Transactions on Industrial Electronics*, vol. 60, no. 6, pp. 2401–2409, 2013.
[14] R. Blasco-Gimenez, N. Aparicio, S. Ano-Villalba, and S. Bernal-Perez, "Lcc-hvdc connection of offshore wind farms with reduced filter banks," *IEEE Transactions on Industrial Electronics*, vol. 60, no. 6, pp. 2372–2380, 2013.
[15] S. Bernal-Perez, S. Ano-Villalba, R. Blasco-Gimenez, and N. Aparicio, "Connection of off-shore wind power plants to vsc-mtdc networks using hvdc diode-rectifiers," in *Industrial Electronics (ISIE), 2013 IEEE International Symposium on*. IEEE, 2013, pp. 1–6.
[16] S. Añó-Villalba, R. Blasco-Gimenez, S. Bernal-Perez, and E. Belenguer, "Wind power plant integration in voltage source converter hvdc grids with voltage droop control," *Mathematics and Computers in Simulation*, 2017.
[17] C. Prignitz, H.-G. Eckel, and S. Achenbach, "Fixref: A current control strategy for offshore wind turbines connected to different types of hvdc transmission," in *Proceedings of the 15th Wind Integration Workshop*, 2016, pp. 1–8.
[18] P. B. Brogan, R. Jones, P. Menke, and R. Zurowski, "Control method for self-commutated converter for controlling power exchange," Aug. 19 2013, uS Patent App. 14/913,182.
[19] P. Kundur, N. J. Balu, and M. G. Lauby, *Power system stability and control*. McGraw-hill New York, 1994, vol. 7.
[20] E.-E. ENTSO-E, "Network code for requirements for grid connection applicable to all generators (nc rfg), march 2013.[online]. available: h ttp," *networkcodes. entsoe. eu/connectioncodes*.
[21] M. A. Cardiel-Alvarez, J. L. Rodriguez-Amenedo, S. Arnaltes, and M. Montilla-DJesus, "Modeling and control of lcc rectifiers for off-shore wind farms connected by hvdc links," *Energy Conversion, IEEE Transactions on*, vol. 32, no. 4, pp. 1284–1296, 2017.
[22] L. M. Castro, E. Acha, and C. R. Fuerte-Esquivel, "A novel vsc-hvdc link model for dynamic power system simulations," *Electric Power Systems Research*, vol. 126, pp. 111–120, 2015.
[23] X.-F. Wang, Y. Song, and M. Irving, *Modern power systems analysis*. Springer Science & Business Media, 2010.